


**Strong-field ionization of the triplet ground state of O<sub>2</sub>**Tomthin Ngamba Wangjam , Huynh Van Sa Lam , and Vinod Kumarappan <sup>\*</sup>  
*James R. Macdonald Lab, Kansas State University, Manhattan, Kansas 66506, USA* (Received 3 August 2021; accepted 29 September 2021; published 25 October 2021)

Using strong-field ionization as a probe, we observe highly nonperiodic evolution of the spin-rotation wave packet launched by a nonionizing femtosecond pulse in oxygen. The nonperiodicity is readily apparent only in rotationally cold molecules that are pumped with a weak alignment pulse. We show that this behavior is a consequence of the spin-rotation and the spin-spin couplings in the triplet ground state of the neutral molecule. A model that includes these couplings in the field-free Hamiltonian but in neither the alignment nor the ionization step explains most of the observed dynamics, suggesting that neither process depends explicitly on the electronic spin. We also show that the angle dependence of strong-field ionization can be retrieved from the delay-dependent signal even when coupling to spin complicates the rotational dynamics.

DOI: [10.1103/PhysRevA.104.043112](https://doi.org/10.1103/PhysRevA.104.043112)**I. INTRODUCTION**

Laser-induced rotational dynamics following impulsive alignment of linear molecules have been investigated extensively for more than two decades [1–9]. In impulsive alignment, the rotational wave packet can be well described by the time-dependent Schrödinger equation (TDSE) for rigid rotors [3]. For linear molecules, typically, the induced rotational wave packets are periodic because rotational energy levels are regularly spaced [7,10]. Such wave packets have been used extensively to study the angle dependence of strong-field ionization (SFI) of molecules, either by scanning the angle between the alignment axis and the polarization of the ionizing pulse or by analyzing the delay dependence of the ionization rate due to the temporal evolution of the rotational wave packet [11–15].

However, the coupling of rotational motion to other degrees of freedom can introduce nonperiodicity in the wave packet. The simplest example is the centrifugal distortion of molecules in high rotational angular momentum states. Although it is often necessary to include the effects of this distortion in modeling the rotational wave packet [16], it is assumed that the angle-dependent ionization rate is not distorted by the small change in the internuclear separation that results from this distortion. The nonperiodicity introduced by the hyperfine coupling between the electric quadrupole moments of the atomic nuclei and the gradient of the electric field created by the electrons in molecular iodine [17] is another example where rotational dynamics is weakly perturbed. In contrast, the delay-dependent high-harmonic yield of impulsively aligned NO, which was attributed to the spin-orbit coupling in the low-lying <sup>2</sup>Π states, is strongly modulated due to the role of spin dynamics in the high-harmonic generation process [18,19].

Here we report nonperiodic revivals of strong-field ionization of oxygen, which is an open-shell molecule with two

unpaired  $\pi$  electrons in the  $X^3\Sigma_g^-$  electronic ground state. The unquenched total electronic spin angular momentum,  $S = 1$ , should lead to peculiar rotational dynamics compared to closed-shell molecules in <sup>1</sup>Σ ground states such as N<sub>2</sub> and CO<sub>2</sub> [15,20–22]. Recently, a detail study of rotational wave packets expected to be produced by impulsive alignment in triplet oxygen has been investigated theoretically [23]. However, in most past studies [11,21,22,24–32], these peculiar dynamics were not observed, and O<sub>2</sub> could be approximated as a spinless molecule. In this article, we show that rotational dynamics in ground-state O<sub>2</sub> can be highly nonperiodic when the rotational temperature is kept low and the pump is weak enough to limit the rotational wave packet to small values of rotational angular momentum. We impulsively align cold O<sub>2</sub> molecules with the pump and then ionize them using a strong-field probe. We show that the observed nonperiodic behavior is a consequence of spin-rotation and spin-spin couplings in the molecule. We model the rotational dynamics by solving the TDSE using an effective Hamiltonian that includes these couplings. We also use a time-domain approach called ORRCS (orientation resolution through rotational coherence spectroscopy) [15,33] to retrieve the angle-dependent ionization rate. This method has been used to retrieve the angle dependence of SFI [14,15,33,34], high-harmonic generation [35,36], and photoelectron [37] and photofragment momentum distributions [15]. We compare our retrieval result with previous SFI measurements [11] and MO-ADK theory [38,39].

**II. EXPERIMENTAL SETUP**

The experimental setup is similar to the one reported in Ref. [15]. A Ti:sapphire laser produces pulses at a 1-kHz repetition rate with an  $\sim$ 40-fs pulse duration and 1.2-mJ pulse energy at a central wavelength of 800 nm. We split the laser output into alignment and ionizing pulses and recombine them after a computer-controlled delay is introduced between them. The laser compressor gratings are adjusted to get the shortest pulse duration for the ionizing probe, while the alignment

<sup>\*</sup>vinod@phys.ksu.edu

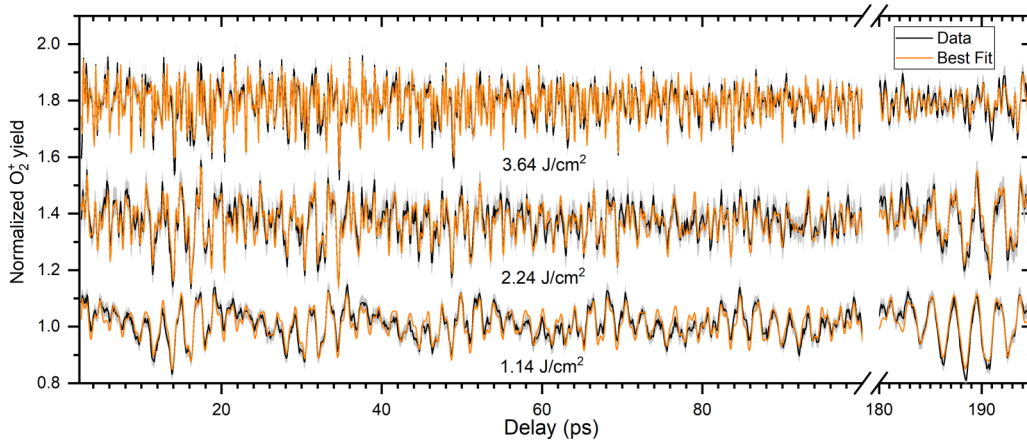


FIG. 1. Delay-dependent normalized  $O_2^+$  yield for different pump intensities (black lines) and their corresponding best fits (orange and gray lines). The probe is the same in all cases, with an intensity of  $260 \text{ TW/cm}^2$ . For clarity, the data and fits for  $2.24$  and  $3.64 \text{ J/cm}^2$  pump fluences are shifted vertically by  $0.35$  and  $0.75$  unit, respectively. The pump fluences estimated from the fits are shown below the corresponding plot lines in the graphs. Statistical error estimates ( $\pm 3\sigma$ ) for the data are shown as light-gray-shaded bands. Data near the end of the scan are shown on an expanded horizontal scale to show detail. The strong nonperiodic behavior is a consequence of the spin-rotation and the spin-spin couplings, as discussed in the text.

pulse is stretched to  $\sim 200$  fs using SF11 glass. Both pulses have the same linear polarization in the plane of the detector of a velocity map imaging spectrometer [40]. An Even-Lavie valve [41], operated with (0.5%) oxygen in helium at a total pressure of 900 psi, generates a rotationally cold ( $T_{\text{rot}} \approx 2$  K) molecular beam target for this experiment.

After the pulses interact with the molecules, we count the number of  $O_2^+$  ions using a velocity map imaging spectrometer equipped with a pair of microchannel plates and a fast P47 phosphor screen. We select  $O_2^+$  ions by gating the microchannel plates so that it is active only when these ions reach it and image the phosphor using a 1000-fps camera (Basler A504k). We determine the centroid of the light intensity on the phosphor for every hit and count the numbers of hits for every laser shot. To avoid any saturation of the measured signal, we use the spectrometer out of focus and record data low count rates ( $\approx 1$  ion per shot).

In order to improve the signal-to-noise ratio, we mechanically chop the alignment beam at 250 Hz, alternately blocking and transmitting pairs of adjacent pulses. The Even-Lavie valve is operated at 500 Hz, so that every alternate pulse in the laser pulse train interacts with the molecular beam. By synchronizing the operation of the chopper and the gas jet using digital delay generators, we create four different combinations of pump, probe, and gas: pump-probe-gas, probe-gas, pump-probe, and probe alone. We label each laser shot with one of these four types and use this information to correct for the fluctuations in laser intensity and gas density. The corrected delay-dependent signal that we use for further analysis is calculated as

$$Y(t) = \frac{Y[\text{Probe, Pump, Gas}] - Y[\text{Probe, Pump}]}{Y[\text{Probe, Gas}] - Y[\text{Probe}]}, \quad (1)$$

where  $Y$  is the count of  $O_2^+$  ions, and  $t$  is the pump-probe delay. Delay scans are repeated multiple times and averaged to minimize the effect of slow drifts under experimental conditions.

The data from three such scans, with different pump pulse energies but otherwise identical conditions, are shown in Fig. 1. In each case, the probe intensity is estimated to be  $260 \text{ TW/cm}^2$  and the pump intensities are  $\sim 2, 4,$  and  $8 \text{ TW/cm}^2$ . The data clearly show not only that the wave packets are nonperiodic, but also that the shape of the revival pattern changes considerably with the intensity of the alignment pulse. The fits to the data shown in Fig. 1 are based on the model discussed below.

### III. MODEL AND ANALYSIS

Compared to the rigid-rotor model used in previous studies [2,3,5,6,15], in this work, we include the spin-rotation and the spin-spin couplings in the ground-state oxygen molecule. The effective field-free Hamiltonian  $H_0$  can be written as

$$H_0 = BN^2 - DN^4 + \frac{2}{3}\lambda(3S_z^2 - S^2) + \gamma \mathbf{N} \cdot \mathbf{S}. \quad (2)$$

The first two terms describe the rotational kinetic energy of molecules, where  $B = 1.4376844 \text{ cm}^{-1}$  is the rotational constant,  $D = 4.87 \times 10^{-6} \text{ cm}^{-1}$  is the centrifugal distortion, and  $\mathbf{N}$  is the rotational angular momentum. The third term describes the spin-spin coupling, where  $\mathbf{S}$  is the electronic spin angular momentum,  $S_z$  is its projection on the internuclear axis, and  $\lambda = 1.98476 \text{ cm}^{-1}$  is the spin-spin coupling constant. The last term describes the spin-rotation coupling where  $\gamma = -0.0084298 \text{ cm}^{-1}$  is the spin-rotation coupling constant. The spectroscopic constants were taken from Ref. [42]. This effective Hamiltonian can successfully reproduce the rotational Raman spectra of  $O_2$  [43–48]. Sonoda *et al.* [23] included neither the centrifugal distortion term nor the off-diagonal terms of the spin-spin coupling in their calculation of spin-dependent dynamics to 20 ps; we keep both to ensure good agreement between measured and modeled quantum beat frequencies for our 200-ps scans [48].

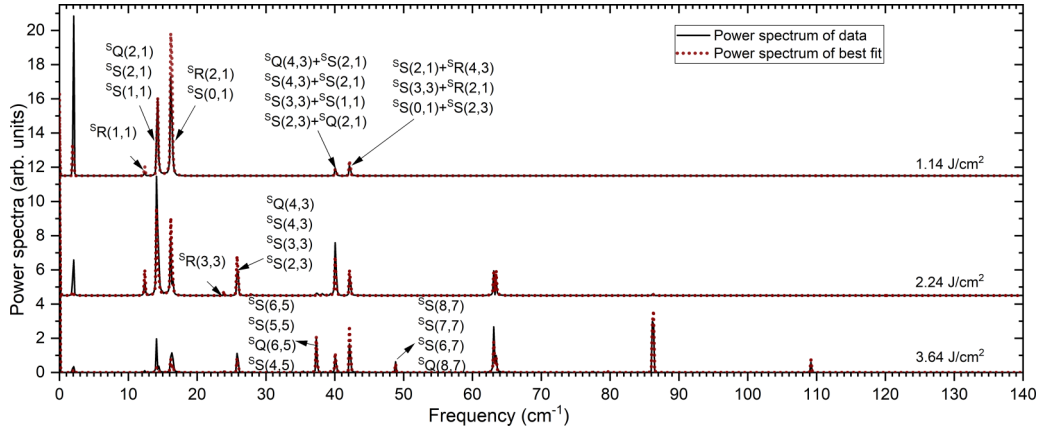


FIG. 2. Fourier spectra of the delay-dependent data (solid black lines) and the best fits (dotted red lines) shown in Fig. 1. We have vertically shifted the spectrum corresponding to 2.24 J/cm<sup>2</sup> by 4.5 units and the one corresponding to 1.14 J/cm<sup>2</sup> by 11.5 units. See text for details of spectroscopic notation and discussion of transition lines.

The interaction between molecules and the alignment pulse can be written as [3]

$$H_{\text{int}}(t) = -\frac{1}{4}\Delta\alpha I(t)\cos^2\theta, \quad (3)$$

where  $\Delta\alpha = 7.13$  atomic units (1 a.u. =  $1.4818 \times 10^{-25}$  cm<sup>3</sup>) [49] is the polarizability anisotropy,  $I$  is the laser intensity, and  $\theta$  is the angle between the molecular axis and the laser polarization. This form of the interaction Hamiltonian implicitly assumes that impulsive alignment is independent of spin. The effective total Hamiltonian is then  $H_{\text{tot}} = H_0 + H_{\text{int}}$ . We model the measured delay-dependent yield  $Y(t)$  as a convolution of the molecular-frame angle-dependent yield,  $S(\theta)$ , and the delay-dependent molecular axis distribution after the pump pulse. Expanding the unknown  $S(\theta)$  in a Legendre polynomial basis with coefficients  $C_L$  leads to

$$Y(t) = \sum_L C_L \langle P_L(\cos\theta) \rangle(t), \quad (4)$$

where  $\langle P_L(\cos\theta) \rangle(t)$  are axis distribution moments—the expectation values of the Legendre polynomials averaged over the thermal distribution of initial states. As described in [15] and [33], we evaluate  $\langle P_L(\cos\theta) \rangle(t)$  from TDSE solutions calculated on a grid of laser intensities, pulse durations, and rotational temperatures.

We then use linear regression to fit  $Y(t)$  to the model described by Eq. (4) over this grid of parameters, and the parameter set that produces the smallest residual sum of squares gives us our best estimate of the spin-rotation wave packet. Simultaneously, we also obtain the angle-dependent yield from the  $C_L$  coefficients, as in Refs. [15,33]. This model assumes that the electron spin plays no explicit role in strong-field ionization; indeed, in theoretical treatments of strong-field ionization electron spin is usually either discounted [50] or not considered at all [38,51] because the optical field does not couple effectively with the spin.

Figure 2 shows Fourier spectra of the data and fits shown in Fig. 1. These spectra show incommensurate frequencies, as expected from the nonperiodic behavior in the time domain. Each data set spans 2.5 to 196.4 ps in pump-probe delay with

a step size of 0.1 ps, sufficient to sample the time evolution of the rotational wave packets and to provide a frequency step size of  $\approx 0.172$  cm<sup>-1</sup>. The insets in both figures provide pump fluences estimated from the fits.

#### IV. RESULTS AND DISCUSSION

Comparing with the rotational Raman spectrum of O<sub>2</sub> [52], we can assign known transitions to the spectral lines in Fig. 2. Without the spin-rotation coupling, there is only one possible Raman transition between any two rotational states [say, the  ${}^S S_0(1, 3)$  transition between  $N = 1$  and  $N = 3$ ] [53]. However, spin-rotation coupling splits each rotational state ( $N$ ) into three states (with the total angular momentum  $J = N, N \pm 1$ ); consequently, the  $\Delta N = 2$  Raman line is split into six. With our experimental resolution, we can only resolve three lines, which are labeled  $S_-(N)$ ,  $S_0(N)$ , and  $S_+(N)$  [52], where the subscript indicates the change in the spin quantum number  $S$ , and  $N$  is the initial rotational angular momentum quantum number. For example, the  $\approx 12$ -cm<sup>-1</sup> line is  $S_-(1)$ . It consists of a single Raman transition,  ${}^S R(1, 1)$ . But the  $S_0(1)$  line at  $\approx 14$  cm<sup>-1</sup> includes  ${}^S Q(2, 1)$ ,  ${}^S S(2, 1)$ , and  ${}^S S(1, 1)$  transitions, and the  $S_+(1)$  line at  $\approx 16$  cm<sup>-1</sup> includes  ${}^S R(2, 1)$  and  ${}^S S(0, 1)$ . Unlike a conventional rotational Raman spectrum, the data also show lines corresponding to multiple Raman cycles (mostly  $\Delta N = 4$ ), as expected in an impulsive alignment experiment [3]. Each of these lines also corresponds to multiple Raman excitation pathways. For instance, the  $\approx 40$ -cm<sup>-1</sup> line comprises four possible excitation pathways, which are shown in Fig. 2. Individual transitions that contribute to the line at  $>60$  cm<sup>-1</sup> are not identified in Fig. 2.

Our data also show a prominent 2-cm<sup>-1</sup> line, which corresponds to  $\Delta N = 0$  and  $\Delta J = 1$  “pure spin” transitions [54,55], in which the spin vector  $\vec{S}$  is reoriented relative to the rotational angular momentum vector  $\vec{N}$ . The presence of this line suggests that both the pump and the probe processes are sensitive to electronic spin. But neither the pump nor the probe step needs to be explicitly dependent on spin for the pure spin line to appear in the fast Fourier transform (FFT) spectrum—the dependence of both on the molecular

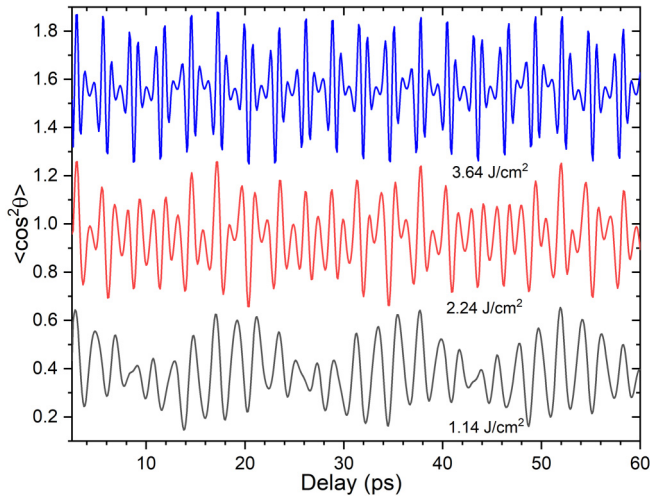


FIG. 3. The expectation value of  $\cos^2\theta$  for spin-rotation wave packets that best fit the data shown in Fig. 1. The plots for 2.24 and 3.64 J/cm<sup>2</sup> fluences were shifted up by 0.5 and 1.1, respectively, for visual clarity.

orientation and of the eigenenergies on the spin and rotation is sufficient. Indeed, our model for the pump excitation [Eq. (3)] depends only on the angle between the molecular axis and the laser polarization vector, but the expectation values of  $P_L(\cos\theta)$  that comprise the fit show the pure spin line in the FFT spectrum.

As the pump intensity is increased, the Fourier spectrum (Fig. 2) shows greater contributions from  $\Delta N > 2$  coherences. In oxygen, the spin-rotation coupling is only important for small values of angular momentum [52]. This is consistent with Eq. (2), where the rotation, spin-rotation, and spin-spin terms scale as  $N^2$ ,  $N^1$ , and  $N^0$ , respectively. In our experiment using a cold molecular beam, almost all the molecules are initially in the lowest rotational state ( $N = 1$ , since  $N = 0$  and all even- $N$  states are forbidden by nuclear spin statistics). Moreover, by keeping the pump fluence low, we keep the rotational wave packet limited to small values of  $N$ . Under these conditions, the dynamics are quite different from the simple periodic behavior expected from a rigid linear rotor. If the initial temperature of the gas sample is high or the alignment pump pulse is strong, the rotational wave packet will be dominated by high- $N$  states and the effect of spin-rotation and spin-spin couplings will be difficult to discern. The effect of the pump fluence can be seen in Fig. 3, in which the expectation values of  $\cos^2\theta$  from the simulations are plotted. Only at the highest fluence does the revival pattern resemble the structure familiar from spinless diatomic molecules. For these reasons, earlier experiments on the SFI of oxygen were not sensitive to the triplet nature of its ground state [21,28,29,32].

Figure 4 shows the angle-dependent ionization rates that we retrieve from the fits. The axis distribution moment of order  $L$  in Eq. (4) arises from transitions with  $\Delta N = L$ . For all three data sets, we truncate the series expansion in Eq. (4) at  $L = 4$  since the  $\Delta N = 6$  contribution is very weak in all three cases, as can be seen in the Fourier spectra of the data; for details see [15] and [33]. The extracted ionization rates in Fig. 4 are in reasonable agreement with MO-ADK calculations and the measurement by Pavičić *et al.* [11].

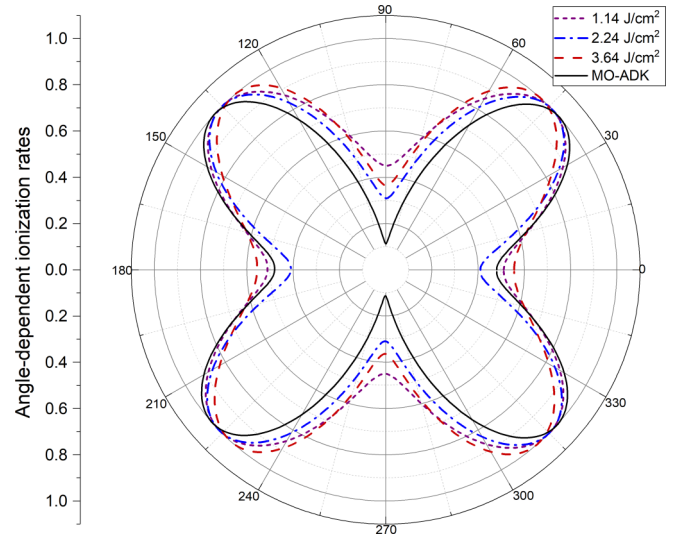


FIG. 4. Angle-dependent ionization rates retrieved from data shown in Fig. 1 and calculated using MO-ADK. In each case, the angle-dependent ionization rate is normalized to its maximum value.

However, as can be seen in Fig. 2, our model accounts very well for the frequencies observed in the experiment, but not for their amplitudes. In our measurements, the average uncertainty of the data is about 1%. For other linear molecules, such as CO<sub>2</sub>, the ORRCS procedure provides excellent fits, with the reduced chi-squared  $\chi_{\text{red}}^2 \approx 1$  [15], indicating a discrepancy between data and fit of the order of the experimental uncertainty. In this work, our fits are not as good as reported before [15], with  $\chi_{\text{red}}^2 \approx 5$ –10. The mismatch can come from two assumptions that we have made in our model: that the initial distribution of molecules is thermal and that SFI does not depend explicitly on the spin. We believe that a nonthermal distribution of initial states is the reason for the mismatch. Previous studies on oxygen seeded in a helium jet [56–58] have found nonthermal distributions of rotational states, suggesting that this is the case in our jet as well. Our setup provides cold molecules at roughly the same temperature as the experiments on O<sub>2</sub> performed by Aquilanti *et al.*, at about 1.8 K [56]. Although better characterization of the initial state distribution can be expected to improve the fits and lead to a more consistent determination of the angle-dependent ionization rate, these measurements demonstrate that the ORRCS method can be used to retrieve the dependence of ultrafast optical processes on molecular alignment even in the presence of coupling of rotations to other degrees of freedom.

## V. CONCLUSIONS

We have measured the nonperiodic evolution of the SFI yield after impulsive alignment of rotationally cold oxygen molecules in a pump-probe experiment. This behavior is a consequence of the spin-rotation and the spin-spin couplings in the triplet ground state of the molecule. Although both rotational and Raman spectroscopy of O<sub>2</sub> are well studied and understood, no signature of this structure has been measured in the SFI experiments to the best of our knowledge. The most important reason for this situation is that spin-spin and spin-



rotation coupling terms do not scale up with the rotational quantum number as rapidly as the rotational energy. Thus, the effect of these couplings is obscured in typical impulsive alignment experiments that use higher initial temperatures and stronger pump pulses. An effective Hamiltonian that includes these couplings accounts for all the frequencies seen in the FFT of the delay-scan data, but it does not fully represent the observed dynamics. This discrepancy is likely to be due to a nonthermal population distribution in our supersonic jet.

High-resolution FFT spectroscopy reveals couplings between rotational motion and other degrees of freedom in molecules. Although oxygen is unusual in having a triplet ground state, coupling of rotation to orbital and spin angular momenta is commonplace in excited states of molecules. Since the rotational constants depend not only on the electronic state but also on individual vibrational levels, FFT spectroscopy of momentum distributions also allows unambiguous identification of long-lived coherences excited by the pump pulse. Although neither the pump nor the probe processes are expected to be explicitly spin dependent in our

experiment, we can nevertheless probe spin dynamics due to the inherent coupling of spin and rotation in the molecule. Such measurements in excited and ionic states of diatomic molecules can be expected to provide us with highly detailed information about the nature of pump-induced wave packets. Strong-field ultrahigh-resolution FFT spectroscopy has been used to measure the rovibrational spectra of  $D_2^+$  [59] and spin-orbit splitting in rare gas atoms [60]. Our results show that such measurements not only yield spectroscopic information about the states populated coherently by the pump pulse, but also help characterize the interaction of the molecule with the probe pulse.

#### ACKNOWLEDGMENTS

We would like to thank C. Bлага, S. Hosseini-Zavareh, and E. Mullins for their help with the laser. This work was supported by the Chemical Sciences, Geosciences, and Biosciences Division, Office of Basic Energy Sciences, Office of Science, US Department of Energy under Award No. DE-FG02-86ER13491.

- 
- [1] B. Friedrich and D. Herschbach, *Phys. Rev. Lett.* **74**, 4623 (1995).
- [2] J. J. Larsen, H. Sakai, C. P. Safvan, I. Wendt-Larsen, and H. Stapelfeldt, *J. Chem. Phys.* **111**, 7774 (1999).
- [3] T. Seideman, *J. Chem. Phys.* **115**, 5965 (2001).
- [4] F. Rosca-Pruna and M. J. J. Vrakking, *Phys. Rev. Lett.* **87**, 153902 (2001).
- [5] H. Stapelfeldt and T. Seideman, *Rev. Mod. Phys.* **75**, 543 (2003).
- [6] J. P. Cryan, P. H. Bucksbaum, and R. N. Coffee, *Phys. Rev. A* **80**, 063412 (2009).
- [7] S. J. Yun, C. M. Kim, J. Lee, and C. H. Nam, *Phys. Rev. A* **86**, 051401(R) (2012).
- [8] S. Pabst, *Eur. Phys. J.: Spec. Top.* **221**, 1 (2013).
- [9] C. P. Koch, M. Lemeshko, and D. Sugny, *Rev. Mod. Phys.* **91**, 035005 (2019).
- [10] T. Seideman, *Phys. Rev. Lett.* **83**, 4971 (1999).
- [11] D. Pavičić, K. F. Lee, D. M. Rayner, P. B. Corkum, and D. M. Villeneuve, *Phys. Rev. Lett.* **98**, 243001 (2007).
- [12] S. Petretti, Y. V. Vanne, A. Saenz, A. Castro, and P. Decleva, *Phys. Rev. Lett.* **104**, 223001 (2010).
- [13] V. P. Majety and A. Scrinzi, *Phys. Rev. Lett.* **115**, 103002 (2015).
- [14] P. Sándor, A. Sissay, F. Mauger, P. M. Abanador, T. T. Gorman, T. D. Scarborough, M. B. Gaarde, K. Lopata, K. J. Schafer, and R. R. Jones, *Phys. Rev. A* **98**, 043425 (2018).
- [15] H. V. S. Lam, S. Yarlagadda, A. Venkatachalam, T. N. Wangjam, R. K. Kushawaha, C. Cheng, P. Svihra, A. Nomerotski, T. Weinacht, D. Rolles, and V. Kumarappan, *Phys. Rev. A* **102**, 043119 (2020).
- [16] D. W. Broege, R. N. Coffee, and P. H. Bucksbaum, *Phys. Rev. A* **78**, 035401 (2008).
- [17] E. F. Thomas, A. A. Søndergaard, B. Shepperson, N. E. Henriksen, and H. Stapelfeldt, *Phys. Rev. Lett.* **120**, 163202 (2018).
- [18] P. M. Kraus, S. B. Zhang, A. Gijbetsen, R. R. Lucchese, N. Rohringer, and H. J. Wörner, *Phys. Rev. Lett.* **111**, 243005 (2013).
- [19] S. B. Zhang, D. Baykusheva, P. M. Kraus, H. J. Wörner, and N. Rohringer, *Phys. Rev. A* **91**, 023421 (2015).
- [20] I. V. Litvinyuk, K. F. Lee, P. W. Dooley, D. M. Rayner, D. M. Villeneuve, and P. B. Corkum, *Phys. Rev. Lett.* **90**, 233003 (2003).
- [21] K. Miyazaki, M. Kaku, G. Miyaji, A. Abdurrouf, and F. H. M. Faisal, *Phys. Rev. Lett.* **95**, 243903 (2005).
- [22] T. Kanai, S. Minemoto, and H. Sakai, *Nature (London)* **435**, 470 (2005).
- [23] K. Sonoda, S. Fukahori, and H. Hasegawa, *Phys. Rev. A* **103**, 033118 (2021).
- [24] J. Itatani, D. Zeidler, J. Levesque, M. Spanner, D. M. Villeneuve, and P. B. Corkum, *Phys. Rev. Lett.* **94**, 123902 (2005).
- [25] V. G. Stavros, E. Harel, and S. R. Leone, *J. Chem. Phys.* **122**, 064301 (2005).
- [26] J. Huang, C. Wu, N. Xu, Q. Liang, Z. Wu, H. Yang, and Q. Gong, *J. Phys. Chem. A* **110**, 10179 (2006).
- [27] Z. Yang and X. Zhou, *Acta Phys.-Chim. Sin.* **22**, 932 (2006).
- [28] F. H. M. Faisal, A. Abdurrouf, K. Miyazaki, and G. Miyaji, *Phys. Rev. Lett.* **98**, 143001 (2007).
- [29] K. Yoshii, G. Miyaji, and K. Miyazaki, *Rev. Laser Eng.* **36**, 1012 (2008).
- [30] A. Korobenko, A. A. Milner, and V. Milner, *Phys. Rev. Lett.* **112**, 113004 (2014).
- [31] P. Peng, Y. Bai, N. Li, and P. Liu, *AIP Adv.* **5**, 127205 (2015).
- [32] G. Kaya, N. Kaya, J. Strohaber, N. A. Hart, A. A. Kolomenskii, and H. A. Schuessler, in *Exploring the World with the Laser: Dedicated to Theodor Hänsch on His 75th Birthday*, edited by D. Meschede, T. Udem, and T. Esslinger (Springer International, Cham, Switzerland, 2018), pp. 577–595.
- [33] V. Makhija, X. Ren, D. Gockel, A.-T. Le, and V. Kumarappan, [arXiv:1611.06476](https://arxiv.org/abs/1611.06476).

- [34] P. Sándor, A. Sissay, F. Mauger, M. W. Gordon, T. T. Gorman, T. D. Scarborough, M. B. Gaarde, K. Lopata, K. J. Schafer, and R. R. Jones, *J. Chem. Phys.* **151**, 194308 (2019).
- [35] X. Ren, V. Makhija, A.-T. Le, J. Troß, S. Mondal, C. Jin, V. Kumarappan, and C. Trallero-Herrero, *Phys. Rev. A* **88**, 043421 (2013).
- [36] J. Troß, X. Ren, V. Makhija, S. Mondal, V. Kumarappan, and C. A. Trallero-Herrero, *Phys. Rev. A* **95**, 033419 (2017).
- [37] C. Marceau, V. Makhija, D. Platzer, A. Y. Naumov, P. B. Corkum, A. Stolow, D. M. Villeneuve, and P. Hockett, *Phys. Rev. Lett.* **119**, 083401 (2017).
- [38] X. M. Tong, Z. X. Zhao, and C. D. Lin, *Phys. Rev. A* **66**, 033402 (2002).
- [39] S.-F. Zhao, C. Jin, A.-T. Le, T. F. Jiang, and C. D. Lin, *Phys. Rev. A* **81**, 033423 (2010).
- [40] A. T. J. B. Eppink and D. H. Parker, *Rev. Sci. Instrum.* **68**, 3477 (1997).
- [41] U. Even, J. Jortner, D. Noy, N. Lavie, and C. Cossart-Magos, *J. Chem. Phys.* **112**, 8068 (2000).
- [42] J. M. Brown and A. Carrington, *Rotational Spectroscopy of Diatomic Molecules. Cambridge Molecular Science* (Cambridge University Press, Cambridge, UK, 2003).
- [43] K. Altmann, G. Strey, J. G. Hoehenbleicher, and J. Brandmüller, *Z. Naturforsch. A* **27**, 56 (1972).
- [44] M. Tinkham and M. W. P. Strandberg, *Phys. Rev.* **97**, 937 (1955).
- [45] K. W. Brown, N. H. Rich, and J. W. Nibler, *J. Mol. Spectrosc.* **151**, 482 (1992).
- [46] A. A. Milner, A. Korobenko, and V. Milner, *New J. Phys.* **16**, 093038 (2014).
- [47] J. D. Miller, S. Roy, J. R. Gord, and T. R. Meyer, *J. Chem. Phys.* **135**, 201104 (2011).
- [48] T. L. Courtney and C. J. Kliewer, *J. Chem. Phys.* **149**, 234201 (2018).
- [49] T. D. Poulsen, P. R. Ogilby, and K. V. Mikkelsen, *J. Phys. Chem. A* **102**, 8970 (1998).
- [50] J. Muth-Böhm, A. Becker, and F. H. M. Faisal, *Phys. Rev. Lett.* **85**, 2280 (2000).
- [51] O. I. Tolstikhin, T. Morishita, and L. B. Madsen, *Phys. Rev. A* **84**, 053423 (2011).
- [52] M. Brard, P. Lallemand, J. P. Cebe, and M. Giraud, *J. Chem. Phys.* **78**, 672 (1983).
- [53] The spectroscopic notation is  $^{\Delta N}\Delta J(N'', J'')$  for a transition from  $(J'', N'')$  to  $(J', N')$ . Letters used for the change in quantum numbers are  $S = +2$ ,  $R = +1$ , and  $Q = 0$ . For instance,  $^S R(1, 1)$  denotes the  $(J' = 2, N' = 3) \leftarrow (J'' = 1, N'' = 1)$  transition.
- [54] D. L. Renschler, J. L. Hunt, T. McCubbin, and S. Polo, *J. Mol. Spectrosc.* **31**, 173 (1969).
- [55] A. Owyong, R. A. Hill, and P. Esherick, *Opt. Lett.* **8**, 425 (1983).
- [56] V. Aquilanti, D. Ascenzi, D. Cappelletti, and F. Pirani, *Nature (London)* **371**, 399 (1994).
- [57] V. Aquilanti, D. Ascenzi, D. Cappelletti, and F. Pirani, *J. Phys. Chem.* **99**, 13620 (1995).
- [58] S. Harich and A. M. Wodtke, *J. Chem. Phys.* **107**, 5983 (1997).
- [59] T. Ando, A. Iwasaki, and K. Yamanouchi, *Phys. Rev. Lett.* **120**, 263002 (2018).
- [60] T. Ando, A. Liu, N. Negishi, A. Iwasaki, and K. Yamanouchi, *Phys. Rev. A* **104**, 033516 (2021).